Knowledge discovery in urban environments from fused multi-dimensional imagery

(Invited Paper)

Erzsébet Merényi
Department of Electrical and Computer Engineering
Rice University
Houston, Texas 77005, U.S.A.
Email: erzsebet@rice.edu

Beáta Csathó
Department of Geology
University of Buffalo, SUNY
Buffalo, NY 14260, U.S.A.
Email: bcsatho@buffalo.edu

Kadim Tasdemir
Department of Electrical and Computer Engineering
Rice University
Houston, Texas 77005, U.S.A.
Email: tasdemir@rice.edu

***Abstract*— With all the exciting advances in sensor fusion and data interpretation technologies in recent years, including co-registration, 3-D surface reconstruction, object recognition, spatial reasoning, and more, high-quality detailed and precise segmentation of remote sensing spectral images remains a much needed key componenent in the comprehensive analysis and understanding of surfaces. Urban surfaces are no exception. In fact, urban surfaces can represent more challenge than many other types because of the very large variety of materials concentrated in relatively small areas. Segmentation (unsupervised clustering) or supervised classification based on spectral signatures from multi- and hyperspectral imagery, or based on other multi-dimensional signatures from stacked disparate (multi-source) imagery, provide delineation of materials with various compositional and physical properties in a scene. Such a cluster or classification map lends critical support to further reasoning for accurate identification of surface objects and conditions. It is, therefore, imperative to develop methods whose data exploitation power matches that of the discriminating power of the data acquisition instrument. We present a study of unsupervised segmentation, comparing the performances of ISODATA clustering and self-organized manifold learning on an urban image from a Daedalus multi-spectral scanner and on an AVIRIS hyperspectral image.**

I. Background and objectives

Multi- and hyperspectral imagers, in general, produce fused data from several regions of the electromagnetic (EM) spectrum, typically Visible, Near-IR and Mid-IR, where the measured physical quantity is reflectance, and sometimes also from Thermal IR, where thermal emission is measured. Each of these windows has diagnostic power for various materials. These data can also be fused with signals acquired in other parts of the EM spectrum, which reflect completely different physical properties (for example, passive microwave, radar) and thus can be preferentially diagnostic of material properties that other windows may not be sensitive to, or have complementary information of. Such fused data are immensely rich. We take the view that for optimal exploitation — *i.e.,* to discriminate classes to the extent the sensor makes possible — one should use all available spectral bands together in clustering or classification. This approach requires powerful techniques, given the large number of relevant classes in an urban scene, with many of them potentially very small, thus statistically insignificant in a large image. For images with several hundred bands the high dimensionality of the data vectors doubles the challenge. Many of the available popular segmentation and classification techniques severely underperform on such data, failing to make important discoveries, or unable to discriminate subtle but consistent spectral differences that sometimes distinguish quite different materials.

Spectral properties of man-made materials, including most objects in urban scenes are known to be complex (*e.g.,* [1], captured only by high spectral resoluion (hyperspectral) imaging. Several recent studies focus on developing methods to exploit such data for precise mapping of urban environments. Good examples include model-based mixture supervised classification [2], feature extraction with mathematical morphology [3], spatial reclassification [4], feature-level fusion of hyperspectral imagery with LIDAR and aerial photography [5], and multigrid Gibbs distribution based partitioning [6]. These provide robust segmentations but often use a significantly reduced number of bands and consequently find less number of classes than exist in the data. New approaches, taking advantage of the full spectral resolution are needed, to identify as many classes as the sensor can discriminate, and to increase the chance of discovery of rare classes.

We present Self-Organizing Map (SOM) based clusterings and classifications that stand to these challenges due to advanced augmentations to the basic Kohonen SOM [7]. We present segmentation studies of urban scenes, from data acquired by different sensors. Since automation of mapping — the production of thematic and other maps from combination of images and other data — is a major goal, and the use of supervised classification can reduce the degree of automation under many circumstances, one objective of this work is to show the high degree of detail that we can achieve with unsupervised segmentation. Another objective is to demonstrate how new knowledge about urban scenes is revealed from fused data sets by the use of this sophisticated approach.

1-4241-4244-0712-5/07/$20.00

A. SOMs and advanced versions

The Self-Organizing neural network paradigm was invented in the early 80's by Teuvo Kohonen [7]. It is an adaptive vector quantization where the quantization prototypes (the weights of the neurons) are anchored to the grid cells of a rigid (usually) two-dimensional lattice. During an iterative unsupervised learning process the prototypes (which have the same dimensionality as the data vectors) are adjusted and become optimally distributed in data space, to collectively best represent the unknown density distribution of the input data. The number of prototypes is given by the lattice size but no assumption is required about the number of clusters. The unique nature of the SOM, compared to other vector quantization methods, is that the prototypes also become spatially ordered on the rigid lattice according to their similarity relationships: the closer two prototypes are in data space the closer they should be in the SOM lattice and vica versa. This ordered layout of a (correctly) learned SOM facilitates, in the SOM lattice, the detection of spatially contiguous groups of prototypes that represent clusters of similar data vectors. This is a two-stage clustering: after the quantization phase, the SOM prototypes are grouped, and all data points that are mapped to one distinct group (one cluster) of prototypes will then be assigned to one data cluster. Such two-stage clusterings have the advantage of reduced noise after the first (quantization) stage, and faster clustering of the much smaller number of protoypes than the original data points. However, it is important that this is a topological mapping, which means that the lattice distances of the prototypes are not linearly proportional to their Euclidean distances in data space (which is the measure of their similarity). To see the similarity landscape of the prototypes in the SOM lattice one must evaluate their distances in data space and superimpose on the lattice by some appropriate visualization. Correct (topology preserving) learning involves several issues for which theoretical background can be found in [8], [9], [10]. Some of the more obvious aspects are lattice size and the number of learning step taken. In our analyses 40 x 40 and 60 x 60 SOM grids were used (for the Daedalus and AVIRIS images, respectively), and typically 2 - 6 million learning steps performed for good fine tuning of the SOM.

Detection of the groups of similar protoypes in the SOM lattice can be done either by clustering the prototype vectors by some algorithm, or by semi-manual extraction from a visualization of the SOM's knowledge. Visualization is used more often than clustering algorithms because with clever visualization more information can be displayed and the human expert is more successful in capturing the cluster boundaries in finer detail than can be done with current clustering methods (see, *e.g.,* [11], and a comparison in [12]). Since the invention of the U-matrix [13], many other visualizations were proposed (see an overview in, *e.g.,* [14]). The U-matrix displays the Euclidean distances of the SOM prototype vectors over the SOM lattice, typically averaging the distances to the lattice neighbors and coloring the grid cell of each prototype to a grey level proportional to this average distance, which results in "fences" delineating clusters (see, *e.g.,* [15]). For relatively small data sets with few clusters mapped to a large SOM lattice this works well, but for large data sets with many clusters (such as remote sensing imagery) a moderate size SOM lattice becomes densely populated and no "empty" corridors are left for easy delineation of prototype clusters. (The use of large SOM lattices can be computationally too expensive for high-dimensional data such as hyperspctral images.) Therefore, we have been applying our own modified version of the U-matrix (mU-matrix), which computes the distances of a prototype to all of its lattice neighbors (8 neighbors on a rectangular grid) separately and displays those over each of the lattice borders between neighbors. For the diagonal neighbors this display is reduced to the corner points, nevertheless the information is provided and can be used. This refinement allows us to find as small as 1-prototype clusters (that in turn may represent a small number of data vectors) thus rare data clusters. Some illustration and insight to this can be found in [16]. With semi-manual cluster extraction from the SOM lattice, some prototypes may, however, remain unclustered. This can result from conservative judgement of the human analyst, or from uncertainty because of noise present in the knowledge representation visualized over the SOM.

We have recently proposed a richer visualization than the mU-matrix, called ConnVis, and have been assessing its utility [12]. SOM clustering based on ConnVis is very similar to that of the mU-matrix based clustering in our analyses, therefore we do not show both. Instead, we present a ConnVis based SOM clustering for our first study from a Daedalus multi-spectral scanner image, and a mU-matrix based SOM clustering for our second study from an AVIRIS image. We are developing the ConnVis technique because it shows more promise for automation than the U-matrix based clustering.

The learned SOM can be coupled with a categorization learning neural layer to form an excellent supervised classifier. The preformed clusters (the SOM's own view of the data structure) greatly aid accurate learning of labeled training samples, and subsequent classification of unseen data vectors. Such an SOM-hybrid neural net is fairly easy to train and does very well with relatively few and unevenly distributed training samples for supervised training, which is particulary important in remote sensing (see [17], [18], [19], [20], [21]). We use information theoretically motivated variants of SOMs, which can control the relative size of the SOM lattice areas allocated to clusters found in the data. For example, it is possible to "magnify" the representation areas for rare clusters (without any prior knowledge of their existence or any properties) thus increasing the chance of their detectability from the learned SOM ([22], [16]).

II. Data Analyses

A. Mapping Ocean City from Daedalus data

First we compare analyses of an image of Ocean City, Maryland, obtained in April, 1997 by a Daedalus AADS-1260 multispectral scanner, with 12 channels in the 0.38–1.1

TABLE I
THE COVER TYPES IN THE CLASSIFICATIONS IN FIG 1

Class	Cover type description	# tr
A	parking lot, roof #0	30
B	roof #1 mostly of town houses	79
C	roof #2 mostly of apartment bldg	40
D	roof #3	32
E	divider line on road (paint)	32
F	roof #4, driveway roof #5, metallic	26
G	road between houses, and roofs	24
H	Dirty sea water at houses	20
I	in canals; pool clean ocean/gulf water	72
J	ocean/bay water, likely with suspended sediments and algae	67
K	vegetation #1 around houses	42
L	vegetation #2 around houses	40
M	Dray grass or soil #3 (iron rich)	97
N	vegetation at shoreline and on empty lots	28
O	vegetation #3, yellowish lawn	35
P	Coastal marshland #1	36
Q	Coastal marshland #2	36
R	Sea water in city canals	102
S	dry empty soil	27
T	pier, and decks at houses(wood)	28
U	roof #6	55
V	roof #7	29
W	shadows of houses	48
X	Coastal marshland #3	35
	Total number of training samples	1060

μm and 11–14 μm windows. The image comprises 512 x 512 pixels with a spatial resolution of 1.5 m/pixel at the middle of the swath. No geometric correction was done. For lack of reliable parameters conversion to reflectance was not an option, therefore we worked with the radiance data. Details of the data acquisition are described in [23]. We excluded bands 1 and 2, and the thermal channels for concerns of extreme noise, so this analysis is somewhat conservative and should be regarded as a first step in the exploration of the potentials of these data. Our present study was conducted with bands 3–10. The image was normalized by dividing each spectrum by its Euclidean norm. This cancels linear effects of viewing geometry and terrain while preserving spectral angles. Thus computing the Euclidean distance between two normalized reflectance spectra is equivalent to using inner product distance (the same as the Spectral Angle Mapper uses in ENVI). We first prepared a supervised classification by training an SOM-hybrid neural net with carefully verified training samples of 24 known material classes, summarized in Table I. The resulting class map, in Fig 1, left, was found showing tight correspondence with aerial photographs and field knowledge. The acquisition of the Daedalus images was part of an initiative by the International Society of Photogrammetry and Remote Sensing (ISPRS) to collect a multisensor data set over an urban area [23]. The data, consisting of Daedalus and AVIRIS imagery, high and low altitude photographs and airborne laser scanning (Airborne Topographic Mapper, ATM) were used in several studies to demonstrate different aspects of data fusion (*e.g.,* [24], [25]). Digital elevation models, oriented stereo photographs and orthophotos derived from this multisensor data set as well as field observations served as ground truth for our supervised classification. While these data were sufficient to distinguish between major land cover types (*e.g.,* roofs, vegetation, sea water), they proved insufficient for unique identification of all spectrally different materials (such as roof variants #1, #2 etc.). Such identification would need field spectrometry, which is a logistical challenge since much of the surface is covered by roofs of private houses. This also prevented acquisition of a sufficient number of test samples for a statistically significant, formal accuracy assessment.

Fig 1 compares our "benchmark" supervised classification (24 classes) with an SOM clustering obtained through ConnVis visualization as described in the previous section. The unsupervised clustering clearly finds all supervised classes and, in addition, discovers several new ones. Clusters that were not known as distinct classes at the time of the supervised classification and that were discovered by SOM clustering later, are indicated in ovals of different colors, but they are not included in Table I. While it is fairly obvious that the features in the red and blue ovals are roofs, and the end of the road in the white oval has a different surface paving than the rest of the road, further interpretation of these will require additional field work or study of aerial photos.

The ISODATA algorithm was run in ENVI (ITT Industries, Inc., http://www.ittvis.com/index.asp). It is an iterative clustering in which first a set of initial cluster means is chosen arbitrarily, followed by the classification of each pixel to the closest cluster mean [26]. Then new cluster means are calculated and the pixels are reclassified. This process continues until the number of pixels that change in any class is less than a selected (%) threshold or the maximum number of iterations is reached. We have run the procedure with the default parameters values in ENVI (change threshold = 5%, minimum number of pixels in class = 1, maximum class standard deviation = 1, minimum class distance = 5 and maximum number merge pairs = 2) for a maximum of five iterations. Experiments allowing more iterations and more pairs of clusters to be merged produced no visible change.

Fig. 2, left, shows the resulting 10 ISODATA clusters when the number of cluster centers was allowed between 5 and 10. The 18 clusters in the right image resulted from allowing 10–20 cluster centers. We tried to recolor the randomly assigned ISODATA colors to those in the cluster map in Fig 1 to help visual comparison. This obviously has limits since clusters between maps from two different algorithms are not necessarily the same. For the same reason the labels on the color wedges on each cluster map are different! In the 10-cluster case (Fig 2, left) ISODATA obviously formed superclusters of the clusters in the SOM map. Seven spectrally distinct roof types (clusters

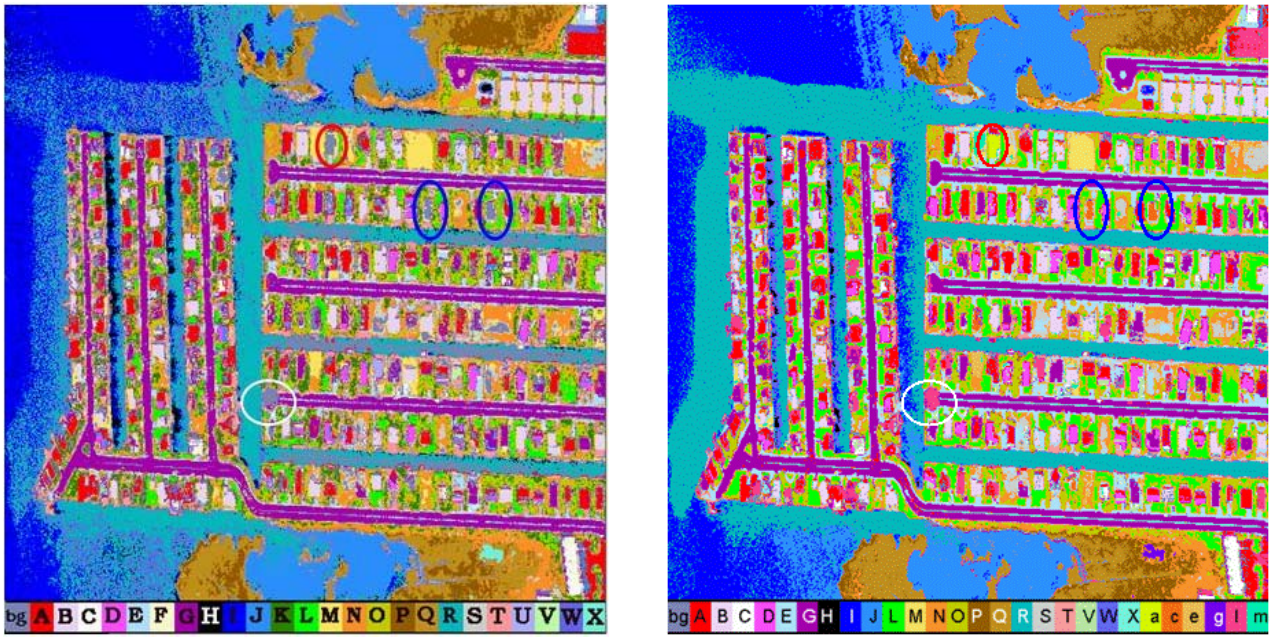

Fig. 1. **Left**: Supervised classification of the Daedalus Ocean City image, mapping 24 known cover types. Red, white and blue ovals show unclassified shapes of buildings and a circle at the end of a road (the colour of the background, bg). **Right**: Clusters identified from a SOM of the Ocean City image, by semi-manual extraction of the cluster boundaries based on ConnVis visualization. The agreement between the cluster map and supervised class map is very good. The apparent difference — the larger amount of green color on the right, compared to the supervised class map — is due to many unclassified pixels in the supervised class map for this rather noisy image, whereas in the cluster map most pixels are assigned to clusters, which produces more appearances of some colours such as green (vegetation) and turquoise (ocean water). The unclassified gray spots (in red, white and blue ovals on the left) are now filled exactly, and with colors different from the 24 colors of the supervised color scheme. Their spectral signatures are distinct from the rest. These newly detected clusters only occur at these locations, indicating the discovery of roof types distinct from the known ones used for the training of the supervised classifier.

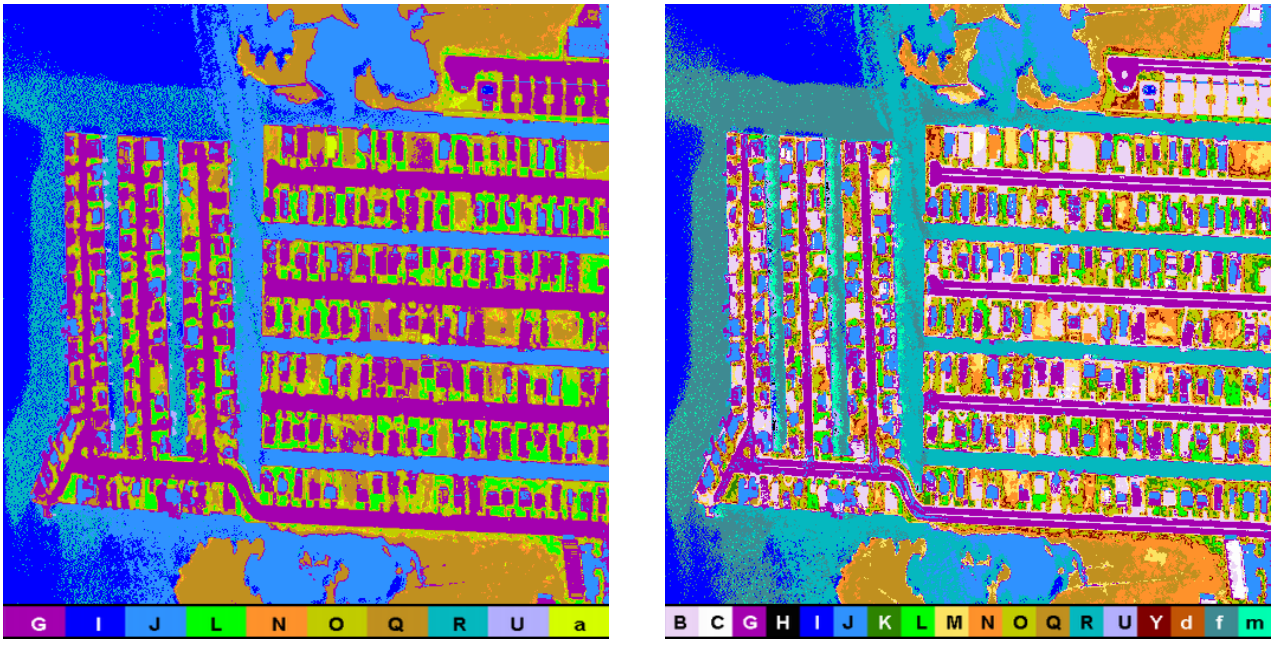

Fig. 2. ISODATA clusterings of the Daedalus Ocean City image. **Left**: 10 clusters resulting from allowing 5 – 10 clusters. Examination of detailes reveals that the ISODATA clustering represent quite clean cut superclusters of the SOM clusters, as discussed in the text. **Right**: 18 clusters resulting from allowing 10 – 20 clusters. Here the ISODATA clusters are still forming supergroups of the SOM clusters, but the relationships are less clean cut. The spectral statistics in Figures 3 and 4 provide an insight to, and comparison of cluster separations.

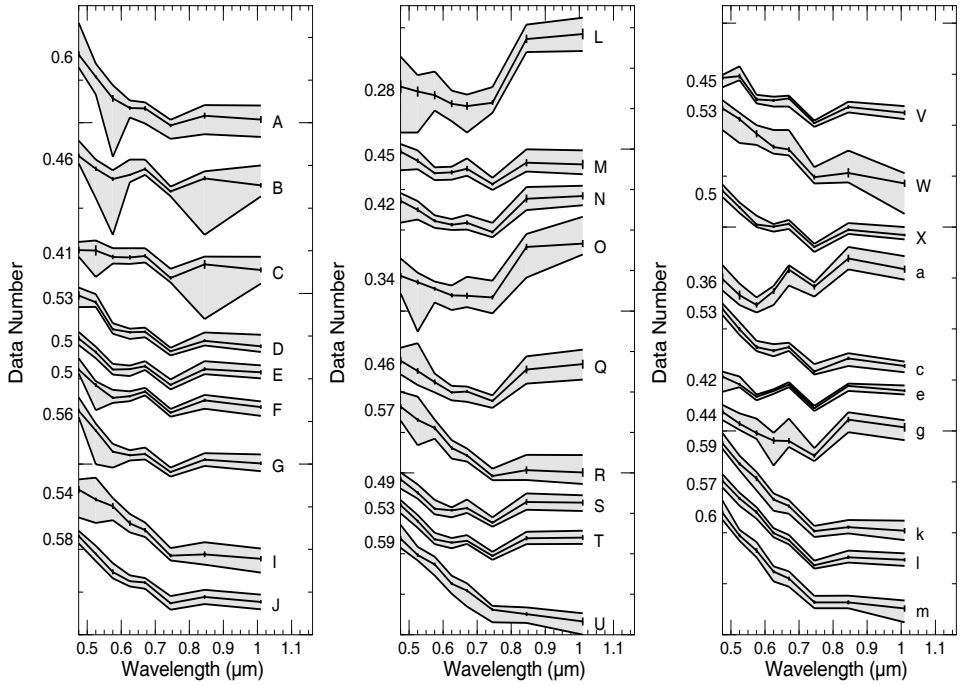

Fig. 3. Spectral statistics of the 28 SOM clusters of the Daedalus image (Fig 1, right). Mean spectra and the envelope of each cluster (shaded area) are displayed, vertically offset for viewing convenience. The number at left of each curve indicates the DN value in the first channel. The standard deviation for all channels are shown by vertial bars.

B, C, D, E, F, U and V) and the concrete roads (G) in the SOM map were put in one ISODATA cluster (G), while SOM cluster A seems to have a match in ISODATA cluster J. However, this ISODATA cluster also maps the water in the bays and canals. Similarly, vegetation groups P, Q, and X, and soil S in the SOM map are contained in ISODATA cluster Q. (Note that X is deep purple in the SOM cluster map, which is the only color inconsistency between the SOM map and the supervised class map.) Clusters N, O and Q (orange, split-pea green, and light brown) are in best correspondence between the two maps. While we cannot state one-to-one match between ISODATA supergroups and SOM groups, given the constraint of maximum 10 clusters ISODATA did a good job. The 18-cluster case (Fig 2, right) is more complicated, but ISODATA still formed recognizable superclusters, albeit a larger number of them. (We can see this not only from the cluster maps shown here, but also from an SOM "recall" of the ISODATA labeled image pixels. The latter means that we check where the labeled samples map in the SOM lattice and how they relate to the SOM clusters.) The correspondence between water bodies is obvious. SOM clusters G (road) and B (roof #1) now have one-to-one match with the same labels in the ISODATA map (altough B in the ISODATA map also includes the divider paint and roof type #4 (E, light blue) and a bare lot (top row of houses). SOM cluster A still maps to ISODATA J, along with part of the D type roofs (the other part of D maps into G), but C corresponds between the two maps. Further scrutiny confirms that the confusion of clusters increased when a larger number of clusters were allowed for ISODATA.

The spectral statistics of the SOM and 18-cluster ISODATA maps, in Figures 3 and 4, provide another way to assess clustering quality. Shown are the mean spectra of the clusters with the standard deviation in each channel indicated by a vertical bar, and the envelope of the cluster (the min/max values for each channel). Small standard deviation along with a tight envelope that generally follows the shape of the mean spectrum (such as for clusters D, E, F, S, T, and others in Fig 3) is convincing of good segmentation. When the envelope is large but the standard deviation is small (such as for clusters A and B in Fig 3) one can assume a few outliers rather than a "loose" cluster. With larger deviations in the channels where the envelope is wide (*e.g.,* cluster C), one may be concerned about cluster confusion. Comparing Figures 3 and 4 one can see that the SOM clustering is tighter and cleaner.

Visual comparison of both the spatial maps of the clusters and the attendant spectral signatures is important in assessing clustering success. The previous example, however, illustrates that it becomes rather difficult as the number of clusters increases. Partly for this reason, one would like to use more objective, and more automated measures as well. Tables II and III present two popular and well established cluster validity indices for the cluster maps shown in Fig 1 and Fig 2.

Cluster validity indices, in general, reward a segmentation

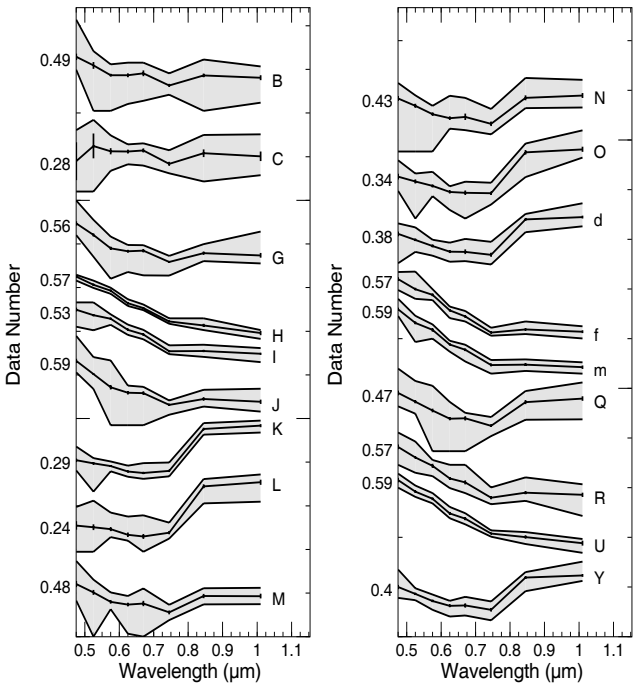

Fig. 4. Spectral statistics of the 18 ISODATA clusters of the Daedalus image (Fig 2, right). Mean spectra and the envelope of each cluster (shaded area) are displayed, vertically offset for viewing convenience. The number at left of each curve indicates the DN value in the first channel. Standard deviation is shown by vertial bars for all channels.

according to what extent it is true that data points in a cluster are more similar to one another than to data points in any other cluster. All indices combine, in some way, a "compactness" (or "scatter") and a "separation" quantity. The former measures how tight a cluster is in terms of its members being similar to one another; the latter measures how dissimilar the clusters are. The sensitivity of the index depends on what information is used about the data points (for example, distances or densities), what distance metrics are used for (dis)similarity (*e.g.,* average of k nearest neighbors, or maximum within cluster distance for similarity; centroid or single linkage distance for cluster dissimilarity), and what quantities are computed to formulate the index (*e.g.,* ratio of "compactness" and "separation"). Two major families of indices are those that are computed from distances between data points, and those that use (in addition or alone) some density measure. For literature on cluster validity indices we refer the reader to [27], [28]. One can measure clustering quality not only from the data directly, but from a clustering of the quantization prototypes, in case of prototype based clustering methods such as mU-matrix and ConnVis clustering of SOM prototypes. Computation of indices from prototypes is at a much reduced expense compared to obtaining the same indices from data points. In the tables below, the Davies-Bouldin Index [29] (DBI) and the Generalized Dunn Index [30], [27] (GDI) are distance based indices. Conn_Index [28] is based on data densities local to the quantization prototypes, through the use of a "connectivity matrix" [12], and is only applicable to prototypes, not to the data vectors directly. Therefore we can use it for the clusterings that were produced from the SOM prototypes. We can also run the ISODATA clusters (the data labeled by ISODATA clustering) through our learned SOM and get an ISODATA label assignment for each SOM prototype. By computing the validity indices for these "ISODATA labeled" prototypes we get a comparison of the SOM and ISODATA clustering on the prototype level. Conn_Index and its two components for "compactness" and "separation", Intra_Conn and Inter_Conn, are under development [28]. We are evaluating the performance of these new indices against the popular indices because the latter seem unreliable for data of high complexity. Table II shows indices computed directly from data points, whereas in Table III indices were computed from the SOM prototypes (as labeled by mU-matrix, ConnVis, and ISODATA clusterings). One obvious difficulty with cluster validity indices is how to interpret the numerical differences. The range of DBI and GDI values is $[0, \infty]$, while Conn_Index and its components have values in $[0, 1]$. It is unclear how to map the range of one index to the range of another, even when they have the same range (such as the DBI and GDI). Therefore, we only make the relative comparison that a clustering is "better" or "worse" than another according to the values that the same index assigns to them.

The DBI and the GDI both favor one of the SOM clusterings over the ISODATA clusterings, in Table II as well as in Table III, *i.e.,* regardless whether the indices were computed from data vectors or from SOM prototypes. (We note that from our experiments it seems that in general, and where applicable, the relative ranking by all indices is the same whether we compute from data vectors directly or from SOM prototypes.) It is interesting, however, that the "runner-up" by the DBI index is the 10-cluster ISODATA map, while we know from the discussion of Fig 1 that this is the least accurate of the three cluster maps presented. DBI gives high mark for this clustering because it particularly favors spherical clusters: both the scatter (compactness) and the cluster separation are calculated from distances to cluster centroids. The DBI value will increase (the grade will decrease) with increasing number of clusters if they do not fit the natural partitions of the data. When only a small number of clusters is allowed, the clusters ISODATA produces are relatively closer to spherical even if those clusters do not fit the natural partitions. In contrast, a large number of ill-fitting clusters is less likely to be close to spherical shapes. The GDI chooses the other (mU-matrix) SOM clustering as second best because it computes the ratio of the minimum separation between clusters to the maximum within-cluster scatter (minimum compactness). In this case, the mU-matrix clustering has considerably less number of data points assigned to clusters because of conservative delineation of a number (but not all) of prototype cluster boundaries in the SOM lattice by the human operator. ConnVis clustering, owing to more explicit density information visualized on the SOM, was able

to identify the boundaries more accurately, and add a few small clusters (the ones highlighted in the ovals in Fig 1). This increased the scatter in several larger clusters, and decreased the minimum separation between clusters, resulting in a higher GDI index. DBI did not favor ConnVis over mU-matrix because it averages the maximum ratios of pairwise scatter and separation, therefore, increased scatter and decreased separation for a few clusters has much less impact in this index than on the GDI. We consider the ConnVis clustering better than the mU-matrix clustering, in this particular case. It is also interesting to analyze the prototype based indices in Table III. Similarly to GDI, Conn_Index favors ConnVis clustering. The large Inter_Conn values (≈ 0.5), for ISODATA clusterings indicate many incorrectly clustered data vectors since Inter_Conn ≥ 0.5 means that either prototypes at cluster boundaries are assigned to the wrong cluster or two clusters should be merged [28]. Intra_Conn, the compactness of clusters, strongly depends on the size of the clusters. This effect is somewhat counterbalanced by Inter_Conn, the separation component of Conn_Index: even though Intra_Conn (compactness) is largest for ISODATA (5–10), this case also has the largest Inter_Conn value (*i.e.,* smallest separation), which makes it the worst clustering as measured by the composite Conn_Index.

TABLE II

VALIDITY INDICES FOR CLUSTERINGS OF THE OCEAN CITY DAEDALUS IMAGE. INDICES ARE COMPUTED FROM DATA VECTORS. KEY TO CLUSTERING METHODS: MU-MATRIX: SEMI-MANUAL CLUSTERING FROM MODIFIED U-MATRIX VISUALIZATION OF THE SOM; CONNVIS: SEMI-MANUAL CLUSTERING FROM CONN VISUALIZATION. FOR ISODATA, THE ALLOWED NUMBER OF CLUSTERS IS SHOWN IN PARETHESES. IN EACH CASE THE ACTUAL NUMBER OF RESULTING CLUSTERS IS GIVEN AS $k = xx$. KEY TO VALIDITY INDICES: DBI: DAVIES-BOULDIN INDEX, LOWER VALUE MEANS BETTER CLUSTERING; GDI: GENERALIZED DUNN INDEX; HIGHER VALUE MEANS BETTER CLUSTERING. THE BEST CLUSTERING BY EACH INDEX IS IN BOLD FACE.

	mU-matrix clustering $k = 28$	ConnVis clustering $k = 28$	ISODATA (10–20) $k = 18$	ISODATA (5–10) $k = 10$
Index				
DBI	**1.17**	1.30	1.30	1.19
GDI	0.41	**0.55**	0.17	0.38

B. Mapping Ocean City from AVIRIS data

We present clusterings of another image of Ocean City, acquired by AVIRIS on Nov 5, 1998, at a relatively low altitude of 4000 m, resulting in 3.8 m/px spatial resolution [5]. The image was orthorectified using the direct orientation derived from position and attitude observations recorded by onboard GPS and INS [31]. Radiance measured by AVIRIS was converted to reflectance by Empirical Line Calibration Method using samples collected by an Analytical Spectral Devices field spectrometer over sand and asphalt during the aircraft over-flight. A false color composite in Fig 5 gives a view

TABLE III

VALIDITY INDICES FOR CLUSTERINGS OF THE OCEAN CITY DAEDALUS IMAGE. INDICES ARE COMPUTED FROM THE SOM PROTOTYPES LABELED BY VARIOUS CLUSTERINGS. KEY TO CLUSTERING METHODS: MU-MATRIX: SEMI-MANUAL CLUSTERING FROM MODIFIED U-MATRIX VISUALIZATION OF THE SOM; CONNVIS: SEMI-MANUAL CLUSTERING FROM CONN VISUALIZATION; ISODATA: SOM PROTOTYPES LABELED BY ISODATA CLUSTERED DATA POINTS. FOR ISODATA, THE ALLOWED NUMBER OF CLUSTERS IS IN PARETHESES. IN EACH CASE THE ACTUAL NUMBER OF CLUSTERS IS GIVEN AS $k = xx$. KEY TO VALIDITY INDICES: DBI: DAVIES-BOULDIN INDEX; GDI: GENERALIZED DUNN INDEX; ITRAC: INTRA_CONN, DENSITY BASED MEASURE OF CLUSTER COMPACTNESS; INTRC: INTER_CONN, DENSITY BASED MEASURE OF CLUSTER SEPARATION; CNI: CONN_INDEX, COMPOSED OF INTER_CONN AND INTRA_CONN. FOR DBI AND INTER_CONN, LOWER VALUE MEANS BETTER CLUSTERING; FOR THE REST, HIGHER VALUES MEAN BETTER CLUSTERING. THE WINNER BY EACH INDEX IS IN BOLD FACE.

	mU-matrix clustering $k = 28$	ConnVis clustering $k = 28$	ISODATA (10–20) $k = 18$	ISODATA (5–10) $k = 10$
Index				
DBI	**1.03**	1.17	1.18	1.06
GDI	0.44	**0.63**	0.20	0.13
CnI	0.63	**0.66**	0.51	0.50
ItraC	0.74	0.83	0.83	**0.86**
IntrC	**0.17**	0.21	0.39	0.42

of the south part of Ocean City where the AVIRIS imagery was collected, with white boxes indicating the two subsections that we included in our cluster analysis. An aerial photograph (Fig 6) shows fine details of surface objects in part of the northern boxed area. The spectral image was preprocessed by the same normalization as the Daedalus image, dividing each spectrum by its Euclidean norm. Bands 1–4, 107–116, and 151–169, showing strong atmostpheric attenuation, were excluded from the analysis. Using all remaining 192 spectral bands, we find 35 meaningful clusters, more than from the Daedalus image, and from the AVIRIS signatures we can identify materials more precisely. Algorithmically this is a larger challenge than the Daedalus case.

Two cluster maps are shown for comparison in Figures 7 and 8. We placed the two boxed areas side by side here and enlarged, for better viewing. An SOM clustering based on modified U-matrix visualization is presented in Fig 7. Because of the semi-manual cluster extraction from the SOM lattice, some prototypes may remain unclustered resulting in a number of unclustered pixels, as explained in section I.A.

In contrast to the Daedalus cluster maps, recoloring the ISODATA map to facilitate visual comparison with the SOM map turned out impossible for this AVIRIS case because of the complexity of the cluster structure and because the cluster structure that ISODATA detects is too intermixed with the cluster structure detected by the SOM. Here, we always refer to cluster labels in each map according to its own color scheme. The spectral signatures of the clusters in these two

Fig. 5. Color composite of the south part of Ocean City. AVIRIS bands 55 (0.8749 μm), 35 (0.683 μm), and 19 (0.5468 μm) were combined into RGB.

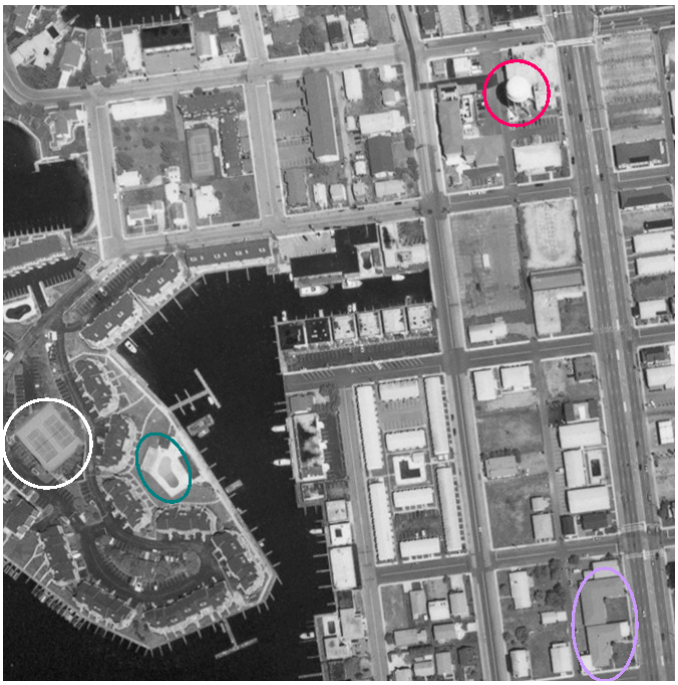

Fig. 6. Aerial photograph of part of the upper boxed area in Fig 5. Circles highlight several objects discussed for their spectral properties: a tennis court (white, cluster C in Fig 7); a fountain in a landscaped area (teal, cluster X); a spectrally unique building (lilac, U); and a water tower (cherry, 'j').

maps are shown (with the respective labels) in Figures 10 and 11. There are a few clusters that show great overlap, such as the sea water, beach sand, vegetation, roads and parking lots (S, e, K-L, I-W-Z-h in the SOM map, and B, E-D, I-J-P, M-K in the ISODATA map, respectively). However, some of these ISODATA clusters contain multiple spectral species, for example, clusters M and K (medium and dark green) map part of the building marked with the single label D (hot pink) in the SOM map. Similarly, the label B (red) in the ISODATA cluster map, which is mostly sea water, also shows on some buildings. One small feature, mapped uniquely by white (C) in Fig 7, left, is a tennis court, which is also well outlined in the ISODATA image but has both I and P signatures. The signature of the SOM cluster C matches quite nicely that of a tennis court signature published by Roberts *et al.,* [32] ("Tennis Court (g)"), whereas the ISODATA cluster signatures I and P have, at best, some slight resemblance to it. This tennis court and a few other objects of interest occur in the northern box in Fig 5, and are also pointed out in an aerial photo in Fig 6.

It is interesting to examine some of the smaller details, annotated in Fig 9, left, in comparison to the ISODATA map (Fig 9, right). These cutouts are from the respective cluster maps of the southern part of Ocean City (from the right images in Figures 7 and 8). The arrows point to the exact same locations in both images, and the white circles enclose the exact same features. The annotations indicate the cluster labels (and thus the cluster colors) associated with the object we discuss. We again remind the reader that the labels in each map are according to that map's color / label wedge. We recommend viewing these maps magnified on a computer screen since 35 colors inevitably include a number of similar ones that may be hard to distinguish in a small size or in a hardcopy, and rare clusters are also hard to see.

Label D on the SOM map indicates a large building and some smaller structures. The spectral signature of these shows a strong iron oxide feature, and can be consistent with the spectrum of a "Dark Roof with Red Gravel", in Roberts *et al.,* [32]. Label V on the left points to a fairly homogeneous spot, which is a miniture golf course, with a unique spectral signature. In the ISODATA map it is not clearly outlined and has three (I,D,K) clusters mixed whose signatures are all different. Cluster V also shows up in a very small spot on the SOM map (circled in white toward the lower right), at the edge of the large parking lot. The actual spectra at these pixel locations indeed match those of the golf course. According to a local map, there are four small structures in a row parallel to the north-south edge of the parking lot, and this V feature is one of them. It appears to be adjacent to a larger building but with a different roof or coating. The ISODATA map assigns its clusters G and S to the same location, both rather flat an featureless spectra and different from the spectra associated with these pixels. In the SOM map the cluster 'a' (greenish-yellow, semi-U shape) is truly unique spectrally (see Fig 7,

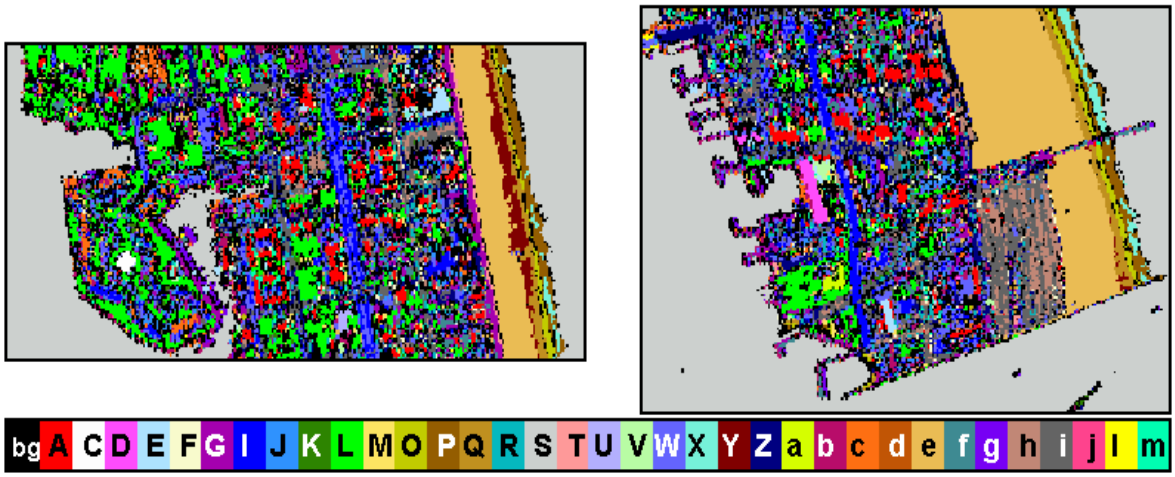

Fig. 7. 35 clusters extracted from mU-matrix visualization of the SOM's knowledge learned from the AVIRIS image of Ocean City. Roads are in the dark blue and medium grey hues (I,J,Z,i), green (K,L) is vegetation, e,O,P,Q map sand layers on the beach, X, S, and P code water. Smaller, unique features are discussed in the text. **Left:** The northern boxed area from Fig 5. **Right:** The southern boxed area from Fig 5. The color 'bg' (black) stands for unclustered pixels.

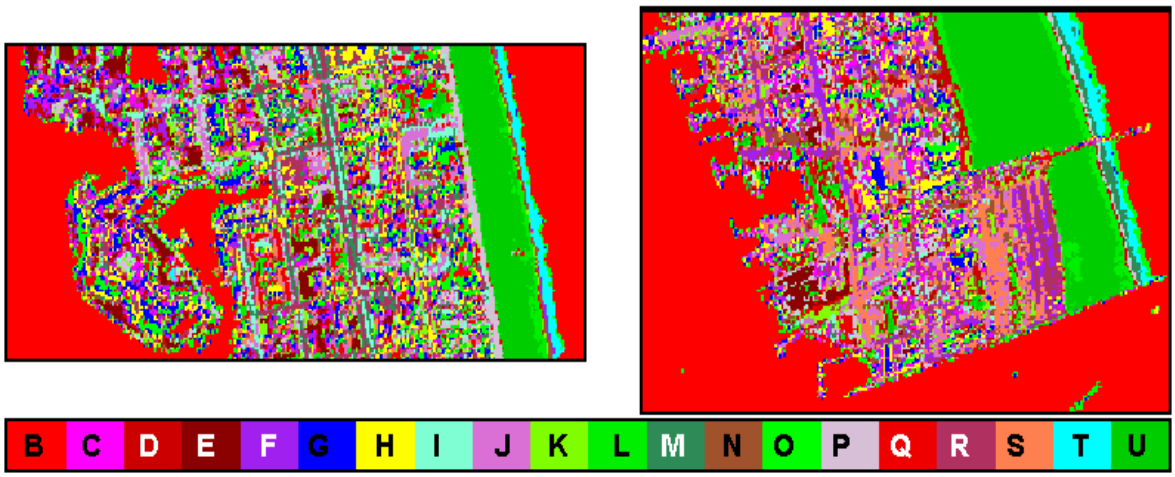

Fig. 8. The 21 clusters produced by ISODATA from the AVIRIS image of Ocean City. **Left:** The northern boxed area from Fig 5. **Right:** The southern boxed area from Fig 5. There are no unclustered pixels.

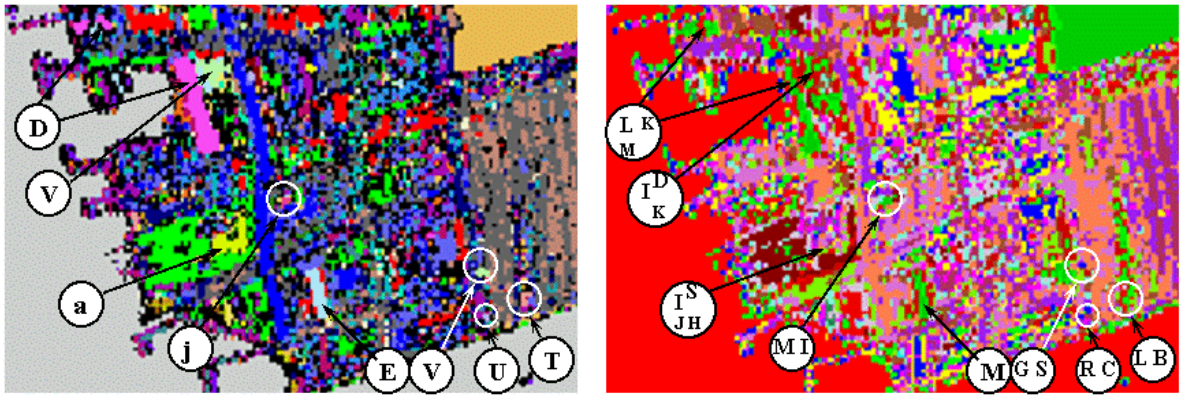

Fig. 9. Details of cluster maps, for a subsection of the south part of Ocean City. **Left:** SOM clusters. **Right:** ISODATA clusters. In both figures, labels and arrows point to the exact same locations. The labels in each figure are given according to their own color / label scheme as keyed in Figures 7 and 8. The selected features are dicussed in the text. Spectral signatures of all clusters are shown in Figures 10 (for SOM) and 11 (for ISODATA), respectively.

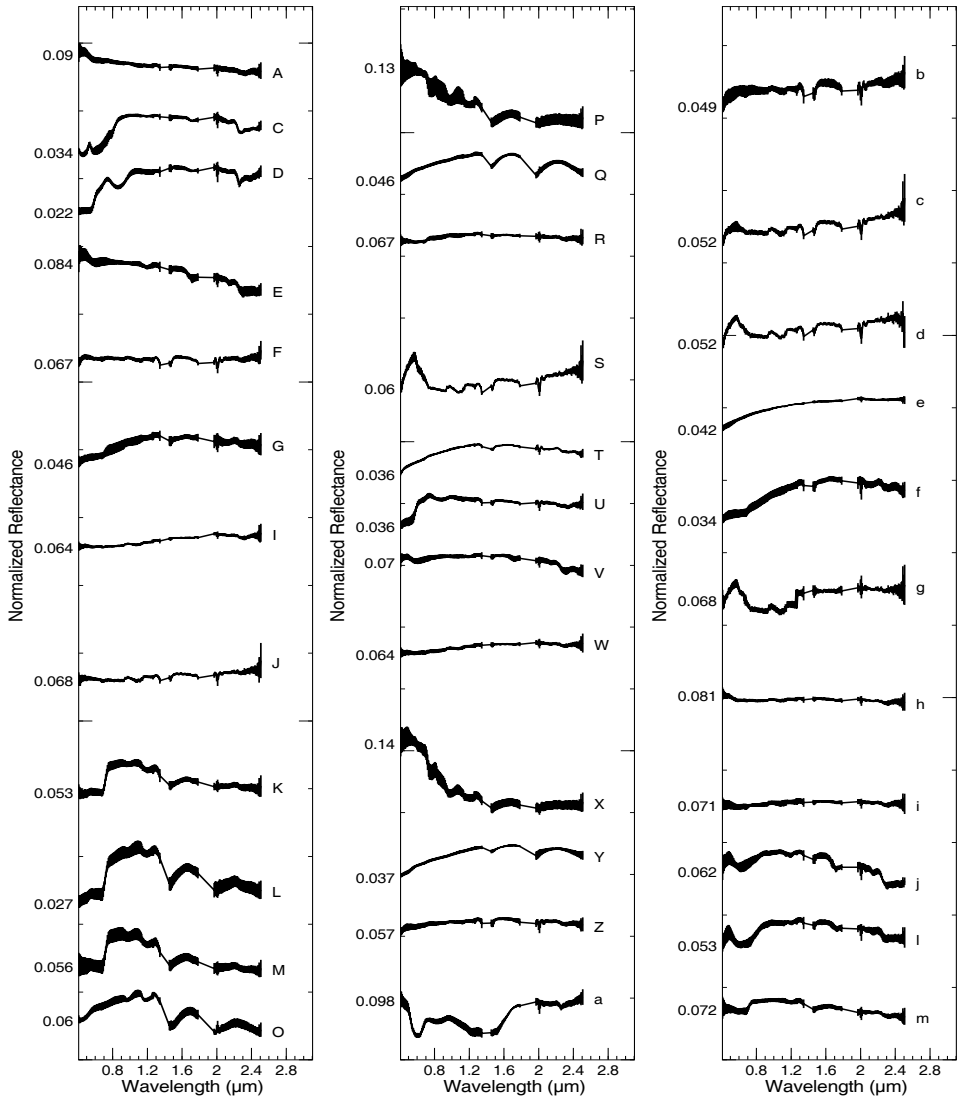

Fig. 10. Spectral statistics of the 35 SOM clusters in Fig 7. Mean spectra are displayed vertically offset for viewing convenience. The number at left is the normalized reflectance value in the first channel. Standard deviation is shown by vertcial bars for all channels. The bare sections of the curves (without standard deviation bars) between approximately 1.3–1.4 μm and 1.9–2.0 μm are windows of data fallout due to saturation of the atmospheric water bands.

Fig 10). It is the roof of the US Coast Guard's building at 610 Philadelphia Ave, and it is very sharply delineated. By informal inquiry with the Coast Guard this is a roof made of a mix of steel and aluminum, painted blue. In the ISODATA map this object is completely obscured by a mix of I,S,J,H clusters, all of them with rather flat spectral signatures. The next annotation marks a tiny object in the SOM map, cluster 'j' in white circle. Again, the spctrum is unique, only found here (about 6 pixels, and at one other location in the north segment (left image in Fig 7) where it is also approximately 6-8 pixels. In both cases this turns out to be a water tower, one of which can be seen in the aerial photo, circled in cherry in Fig 6. In the ISODATA map the same pixels are clusterd with M and I (mostly sand and road material). The long narrow building indicated by the label E (light blue) on the left is mapped by cluster M on the right (the same ISODATA cluster that also covers the beach sand, and the red gravel roof). The tiny, 3-pixel feature labeled U (lilac color) has the exact same spectral signature as one other (larger) building in the northern cutout and encircled in a lilac oval in the aerial photo. It is sharply discriminated from the very different spectral signatures of adjacent pixels, and spatially coincides with a lookout tower of the Coast Guard, therefore we are confident that this is not just noise. The SOM spectrum U is consistent with "Light Red Composite Shingle" in Roberts *et al.,* [32]. ISODATA does not map this building uniquely, and its R and C clusters that show at this location are both quite different from the actual spectra at this location, which look like the mean spectrum of the SOM cluster U. Another small shape that could be a building shows an SOM label T. The corresponding

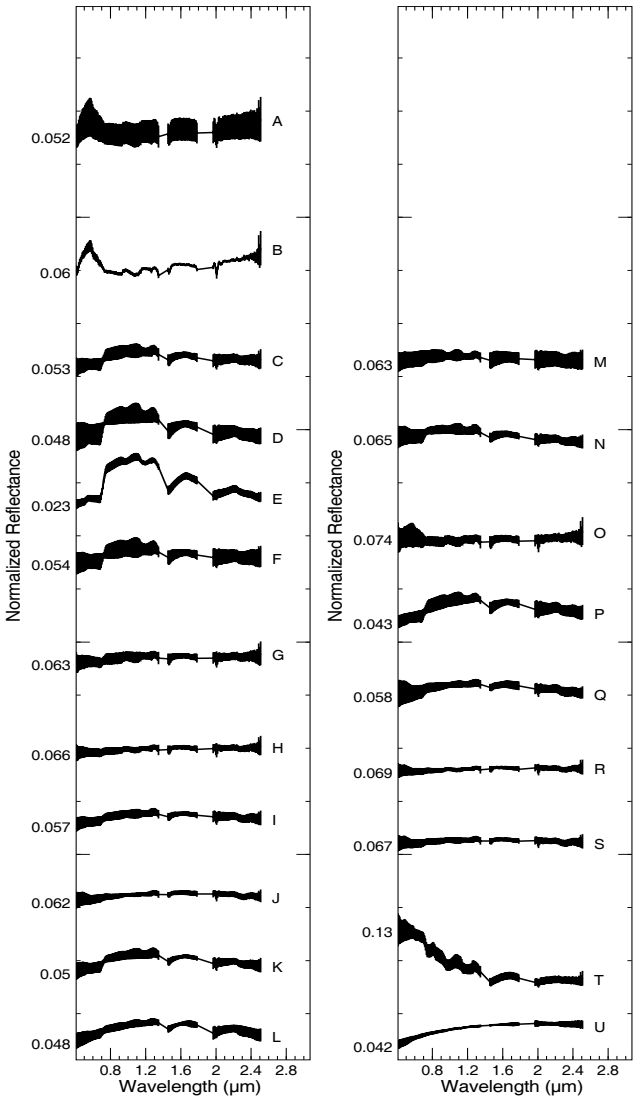

Fig. 11. Spectral statistics of the 21 ISODATA clusters in Fig 8. Mean spectra are displayed vertically offset for viewing convenience. The number at left is the normalized reflectance in the first channel. Standard deviation is shown by vertcial bars for all channels. The sections of curves without standard deviation bars between approximately 1.3–1.4 μm and 1.9–2.0 μm are windows of data fallout due to saturation of the atmospheric water vapor bands.

spectrum is very similar to the "10 Year Red Composite Roof" in Roberts *et al.,* [32]. However, this cluster also shows up as a thin border between town and sand beach in the north segment, where the spectrum is slightly different. ISODATA assigns its L and B clusters to this feature, out of which L is similar to the actual spectra of this feature. One interesting discovery is a small fountain in a landscaped area (in teal colored circle in Fig 6). The few-pixel area belongs to cluster X (water) and is in stark spectral contrast to the surrounding pixels which have the flat signatures of concrete. The entire fountain is embedded in a landscaped grass covered semicirle.

In Figures 10 and 11 the envelopes of clusters are not shown to avoid crowding. While in Fig 10 each mean spectrum is different enough from all others to warrant a separate cluster notice also that the standard deviations suggest fairly homogeneous clusters. The exceptions — somewhat more variable clusters — are the water types (S, X, P), and the vegetation groups (K, L, M). In contrast, a number of the ISODATA mean spectra (Fig 11) are quite similar to one another, and their standard deviations are generally larger than those of the SOM clusters. Conspicuously, none of the truly unique and interesting spectral types were discovered by ISODATA. Interpretation of the spectra of some clusters will take time. We mention a few possibilities in addition to what we already suggested at the discussion of the selected clusters in Fig 9. The SOM cluster 'l' resembles the spectrum of "Blue Street Paint" in [32]. It appears at the tip of piers in small areas, the most prominent example is at the upper left corner of the right image in Fig 7. 'g' (deep purple) and G typically occur together along boardwalks, but the two have very different signatures. G could be wooden material while 'g' has features similar to S and 'd', so it may be a mixed signature of water and underlying materials.

Similarly to the evaluations of the clustering of the Daedalus image, Tables IV and V list validity index values for these AVIRIS clusterings. As with the Daedalus case we have another semi-manual SOM clustering based on ConnVis visualization, which is too similar visually (on the scale of Fig 7) to merit a separate figure, but we include it in the tables of validity indices. Here (contrary to the Daedalus case), we consider the mU-matrix clustering better than the ConnVis clustering because of the discovery of several interesting but very rare clusters by the mU-matrix approach. The number of unclustered pixels is more similar in the two maps in this case than it was for the Daedalus image. Table IV

TABLE IV

VALIDITY INDICES FOR CLUSTERINGS OF THE OCEAN CITY AVIRIS IMAGE. INDICES ARE COMPUTED FROM DATA VECTORS. KEY TO CLUSTERING METHODS: MU-MATRIX: SEMI-MANUAL CLUSTERING FROM MODIFIED U-MATRIX VISUALIZATION OF THE SOM; CONNVIS: SEMI-MANUAL CLUSTERING FROM CONN VISUALIZATION. FOR ISODATA, THE ALLOWED NUMBER OF CLUSTERS IS SHOWN IN PARETHESES. IN EACH CASE THE ACTUAL NUMBER OF RESULTING CLUSTERS IS GIVEN AS $k = xx$. KEY TO VALIDITY INDICES: DBI: DAVIES-BOULDIN INDEX, LOWER VALUE MEANS BETTER CLUSTERING; GDI: GENERALIZED DUNN INDEX, HIGHER VALUE MEANS BETTER CLUSTERING. THE BEST CLUSTERING BY EACH INDEX IS IN BOLD FACE.

	mU-matrix clustering $k = 35$	ConnVis clustering $k = 30$	ISODATA (10–20) $k = 10$	ISODATA (20–30) $k = 21$
Index				
DBI	1.92	**1.63**	5.32	5.50
GDI	**0.20**	0.17	0.15	0.10

shows that DBI strongly favors the SOM clusterings over the ISODATA clusterings, with much larger differences in the

TABLE V

VALIDITY INDICES FOR CLUSTERINGS OF THE OCEAN CITY DAEDALUS IMAGE. INDICES ARE COMPUTED FROM THE SOM PROTOTYPES LABELED BY VARIOUS CLUSTERINGS. KEY TO CLUSTERING METHODS: MU-MATRIX: SEMI-MANUAL CLUSTERING FROM MODIFIED U-MATRIX VISUALIZATION OF THE SOM; CONNVIS: SEMI-MANUAL CLUSTERING FROM CONN VISUALIZATION; ISODATA: SOM PROTOTYPES LABELED BY ISODATA CLUSTERED DATA POINTS. FOR ISODATA, THE ALLOWED NUMBER OF CLUSTERS IS IN PARETHESES. IN EACH CASE THE ACTUAL NUMBER OF CLUSTERS IS GIVEN AS $k = xx$. KEY TO VALIDITY INDICES: DBI: DAVIES-BOULDIN INDEX; GDI: GENERALIZED DUNN INDEX; ITRAC: INTRA_CONN, DENSITY BASED MEASURE OF CLUSTER COMPACTNESS; INTRC: INTER_CONN, DENSITY BASED MEASURE OF CLUSTER SEPARATION; CNI: CONN_INDEX, COMPOSED OF INTER_CONN AND INTRA_CONN. FOR DBI AND INTER_CONN, LOWER VALUE MEANS BETTER CLUSTERING; FOR THE REST, HIGHER VALUES MEAN BETTER CLUSTERING. THE WINNER BY EACH INDEX IS IN BOLD FACE.

	mU-matrix clustering $k = 35$	ConnVis clustering $k = 30$	ISODATA (10–20) $k = 10$	ISODATA (20–30) $k = 21$
Index				
DBI	1.49	**1.26**	5.09	5.50
GDI	0.19	**0.19**	0.16	0.10
CnI	0.63	**0.65**	0.28	0.02
ItraC	0.78	**0.85**	0.56	0.44
IntrC	**0.19**	0.23	0.51	0.94

index values than for the Daedalus image. We interpret this to be the consequence of higher complexity in the natural cluster structure of the AVIRIS data, which ISODATA can match to a lesser degree. mU-matrix is deemed a little worse than ConnVis by DBI, which may be the result of the presence of several very small (low-scatter) but truly unique (well separated) clusters in the mU-matrix clustering, compared to the otherwise very similar ConnVis clustering. GDI is more sensitive to the ratio of the maximum cluster scatter to the minimum pairwise separation between clusters. The maximum scatter may not be much affected by the addition of several tiny clusters, but the minimum separation may change by a perceptible amount. This can explain why GDI favors the mU-matrix clustering over ConnVis. It is harder to explain why GDI has such small difference for ConnVis and ISODATA 10–20. It appears that these indices are not suitable for comparing partitionings on the level of granularity that the number of clusters, the variety of cluster shapes and sizes, and the presence of rare clusters creates. In Table V, DBI and GDI present a similar ranking, and all indices assign higher grades to the SOM clusterings than to the ISODATA ones. Conn_Index and its "compactness" component, Intra_Conn, favor ConnVis clustering over the mU-matrix, even though we know that the mU-matrix partitioning found more natural clusters. Again, this probably has to do with the fact that Intra_Conn only considers densities, thus the addition of very small clusters makes an imperceptible difference in its value. The Inter_Conn (separation) component, however, is more responsive to the inclusion of rare clusters because it computes the relative connectedness (similarity) of the protoypes that are at cluster boundaries, to their own clusters versus to the neighbor clusters, regardless of the number of all prototypes within a cluster (and regardless of how similar those are). These indices, although indicating some of the first order relationships among the presented clusterings, do not seem to capture the relative merits of finer structures.

III. DISCUSSION AND CONCLUSION

The presented studies illustrate an important point: the more complex the data structure the more advantage SOM clustering appears to have over ISODATA (and, from our experience with other hyperspectral data sets, over conventional clustering and classification methods, in general). Using SOM based techniques the full dimensionality needs not be sacrificed because this approach can handle the large number of dimensions with relative ease. Consequently, the full discovery potential afforded by the sensor is retained allowing the detection of many interesting or suprising but spatially small surface features. SOM segmentation and classification can also be applied to stacked disparate data from different sensors.

An SOM is fully automatic in its first stage not requiring a guess of the number of clusters, but semi-manual cluster extraction is needed in its second stage. The discrimination and discovery capability of SOM based clustering is high, but computationally expensive. This can be alleviated by massively parallel hardware implementation of proven SOM-based algorithms. The semi-manual extraction of clusters from the learned SOM is another bottleneck in a production environment. Automation of this second stage on the level of sophistication a human expert can interpret a learned SOM has not been done yet. The knowledge representation we developed for ConnVis visualization captures more information about the SOM than other representations we know of [12]. We are working on utilizing it for full automation.

Development of sophisticated clustering algorithms is incomplete without equally powerful methods for the assessment of the clustering quality. We illustrated some of the issues that hinder such assessment with existing cluster validity indices on a level of reliability that is needed for credible, detailed delineation of urban cover types. We also presented a new cluster validity index that shows promise for complicated data structures, but needs more development based on feedback from studies such as the ones in this paper.

The accuracy assessment of supervised classifications is, in principle, more straightforward, backed by mature works in statistics and sampling theories. Yet an insurmountable problem is presented by data where the stacked data vectors are of very high dimensionality. For such data, because of its capacity to discriminate among many classes, the number of test samples required for statistically significant accuracy assessment can easily be in the thousands for a scene similar to the AVIRIS image we analyzed here. Such requirement can rarely be met, which leaves algorithm developments without

reliable evaluations. High quality synthetic spectral imagery generated by principled simulations, such as the work by Kerekes *et al.,* (this volume) is key to addressing this problem, as well as to supporting the development of intricate unsupervised clustering algorithms.

In conclusion, we believe that the development of powerful analysis techniques, namely advanced "precision" data mining tools, for fused multisensor data sets can greatly contribute toward the detailed mapping of urban environments, and that investment in such developments can have high returns.

ACKNOWLEDGMENT

EM and KT are partially supported by grant NNG05GA94G from the Applied Information Research Program of NASA, Science Mission Directorate. All data were collected as part of an International Society of Photogrammetry and Remote Sensing (ISPRS) initiative to establish standard data sets [23]. We thank Grady Tuell for coordinating the data acquisition campaign and for providing ground spectral measurements for atmospheric correction of the AVIRIS image. Daedalus images and aerial photographs were acquired by the National Geodetic Survey. AVIRIS imagery were provided by NASA JPL. Aerial photographs were digitized at the Digital Photogrammetry Laboratory of the Ohio State University.

REFERENCES

[1] M. Herold, D. A. Roberts, M. E. Gardner, and P. Dennison, "Spectrometry of urban areas for remote sensing – development and analysis of a spectral library from 350 to 2400 nm," *Remote Sensing of Environment*, vol. 91, pp. 304–319, 2004.

[2] M. Dundar and D. Landgrebe, "Toward an optimal supervised classifier for the analysis of hyperspectral data," *IEEE Transactions on Geoscience and Remote Sensing*, vol. 42, no. 1, pp. 271–277, 2004.

[3] J. Benediktsson, J. Palmason, and J. Sveinsson, "Classification of hyperspectral data from urban areas based on extended morphological profiles," *IEEE Transactions on Geoscience and Remote Sensing*, vol. 43, no. 3, pp. 480–491, 2005.

[4] F. Dell'Acqua, P. Gamba, A. Ferrari, J. Palmason, and J. Benediktsson, "Exploiting spectral and spatial information in hyperspectral urban data with high resolution," *IEEE Geoscience and Remote Sensing Letters*, vol. 1, no. 4, pp. 322–326, 2004.

[5] B. Csathó, T. Schenk, and S. Seo, "Spectral interpretation based on multisensor fusion for urban mapping," in *Proc. 2nd GRSS/ISPRS Joint Workshop on Remote Sensing and Data Fusion over Urban Areas, URBAN 2003*, Berlin, May 22–23 2003.

[6] R. Rand and D. Keenan, "Spatially smooth partitioning of hyperspectral imagery using spectral/spatial measures of disparity," *IEEE Transactions on Geoscience and Remote Sensing*, vol. 41, no. 6, pp. 1479–1490, 2003.

[7] T. Kohonen, *Self-Organization and Associative Memory*. New York: Springer-Verlag, 1988.

[8] T. Martinetz and K. Schulten, "Topology representing networks," *Neural Networks*, vol. 7(3), pp. 507–522, 1994.

[9] T. Villmann, R. Der, M. Herrmann, and T. Martinetz, "Topology Preservation in Self–Organizing Feature Maps: Exact Definition and Measurement," *IEEE Transactions on Neural Networks*, vol. 8, no. 2, pp. 256–266, 1997.

[10] L. Zhang and E. Merényi, "Weighted differential topographic function: A refinement of the topographic function," in *Proc. 14th European Symposium on Artificial Neural Networks (ESANN'2006)*. Brussels, Belgium: D facto publications, 2006, pp. 13–18.

[11] J. Vesanto and E. Alhoniemi, "Clustering of the self-organizing map," *IEEE Transactions on Neural Networks*, vol. 11, no. 3, pp. 586–600, May 2000.

[12] K. Tasdemir and E. Merényi, "Data topology visualization for the Self-Organizing Map," in *Proc. 14th European Symposium on Artificial Neural Networks, ESANN'2006, Bruges, Belgium*, Bruges, Belgium, 26-28 April 2006, pp. 125–130.

[13] A. Ultsch, "Self-organizing neural networks for visualization and classification." in *Information and Classification — Concepts, Methods and Applications*, R. K. O. Opitz, B. Lausen, Ed. Berlin: Springer Verlag, 1993, pp. 307–313.

[14] K. Tasdemir and E. Merényi, "Considering topology in the clustering of Self-Organizing Maps," in *Proc. 5th Workshop on Self-Organizing Maps (WSOM 2005)*, Paris, France, September 5–8 2005, pp. 439–446.

[15] M. Kraaijveld, J. Mao, and A. Jain, "A nonlinear projection method based on Kohonen's topology preserving maps," *IEEE Trans. on Neural Networks*, vol. 6, no. 3, pp. 548–559, 1995.

[16] E. Merényi and A. Jain, "Forbidden magnification? II." in *Proc. of European Symposium on Artificial Neural Networks (ESANN'04)*. Bruges, Belgium, April 28-30: D facto publications, 2004, pp. 57–62. [Online]. Available: http://www.ece.rice.edu/∼erzsebet/publist-Merenyi.pdf

[17] E. S. Howell, E. Merényi, and L. A. Lebofsky, "Classification of asteroid spectra using a neural network," *Jour. Geophys. Res.*, vol. 99, no. E5, pp. 10,847–10,865, 1994.

[18] E. Merényi, "Precision mining of high-dimensional patterns with self-organizing maps: Interpretation of hyperspectral images." in *Quo Vadis Computational Intelligence: New Trends and Approaches in Computational Intelligence (Studies in Fuzziness and Soft Computing, Vol 54, P. Sincak and J. Vascak Eds.)*. Physica Verlag, 2000. [Online]. Available: http://www.ece.rice.edu/∼erzsebet/papers/isci00-paper.pdf

[19] E. Merényi, W. H. Farrand, L. Stevens, T. Melis, and K. Chhibber, "Mapping Colorado River ecosystem resources in Glen Canyon: Analysis of hyperspectral low-altitude AVIRIS imagery," in *Proc. ERIM, 14th Int'l Conference and Workshops on Applied Geologic Remote Sensing, 4–6 November, 2000, Las Vegas, Nevada*, 2000.

[20] T. Villmann, E. Merényi, and B. Hammer, "Neural maps in remote sensing image analysis," *Neural Networks*, vol. 16, pp. 389–403, 2003.

[21] L.Rudd and E. Merényi, "Assessing debris-flow potential by using aviris imagery to map surface materials and stratigraphy in cataract canyon, Utah," in *Proc. 14th AVIRIS Earth Science and Applications Workshop*, R. Green, Ed., Pasadena, CA, May 24–27 2005.

[22] E. Merényi, A. Jain, and T. Villmann, "Explicit magnification control of self-organizing maps for "forbidden" data," *IEEE Trans. on Neural Networks*, p. in press, 2007.

[23] B. Csathó, W. Krabill, J. Lucas, and T. Schenk, "A multisensor data set of an urban and coastal scene," in *Int'l Archives of Photogrammetry and Remote Sensing*, vol. 32, no. 3/2, 1998, pp. 26–31.

[24] B. Csathó, , T. Schenk, D.-C. Lee, and S. Filin, "Inclusion of multispectral data into object recognition," in *Int'l Archives of Photogrammetry and Remote Sensing*, vol. 32, no. 7–4–2 W6, 1998, pp. 53–61.

[25] T. Schenk and B. Csathó, "Fusion of lidar data and aerial imagery for a more complete surface description," in *Int'l Archives of Photogrammetry and Remote Sensing*, vol. 34, no. 3A, 2002, pp. 310–317.

[26] J. Tou and R. C. Gonzalez, *Pattern Recognition Principles*. Reading, Massachusetts: Addison-Wesley Publishing Company, 1974.

[27] J. Bezdek and N. Pal, "Some new indexes of cluster validity," *IEEE Trans. System, Man and Cybernetics, Part-B*, vol. 28, no. 3, pp. 301–315, 1998.

[28] K. Tasdemir and E. Merényi, "A new cluster validity index for prototype based clustering algorithms based on inter- and intra-cluster density," in *Proc. Int'l Joint Conf. on Neural Networks (IJCNN 2007)*, Orlando, Florida, USA, August 12–17 2007, p. submitted.

[29] D. Davies and D. Bouldin, "A cluster separation measure," *IEEE Trans. Pattern Analysis Machine Intelligence (PAMI)*, vol. 1, no. 2, pp. 224–227, 1998.

[30] J. Dunn, "Well separated clusters and optimal fuzzy partitions," *J. Cybernetics*, vol. 4, pp. 95–104, 1974.

[31] J. Boardman, "Precision geocoding of low altitude AVIRIS data: lessons learned in 1998," in *Proc. 8th AVIRIS Earth Science and Applications Workshop*, Pasadena, CA, February 8-11 1999.

[32] D. Roberts, M. Gardner, B. Powell, P. Dennison, and V. Noronha, "Mapping roads and other urban materials using hyperspectral data," in *Proc. Road CenterLine Extraction & Maintenance Specialist Meeting*, Santa Barbara, CA, 6–7 August 2001. [Online]. Available: http://www.ncgia.ucsb.edu/ncrst/meetings/clem2001